In Vitro Cytotoxicity of ^{211}At-Astatide and ^{131}I-Iodide to Glioma Tumor Cells Expressing the Sodium/Iodide Symporter

Sean Carlin, PhD; Gamal Akabani, PhD; and Michael R. Zalutsky, PhD

Department of Radiology, Duke University Medical Center, Durham, North Carolina

The sodium/iodide symporter (NIS) has been identified as an attractive target for cancer therapy. The efficacy of ^{131}I-iodide for NIS-expressing tumor therapy may be limited by a combination of poor cellular retention and unfavorable physical characteristics (long physical half-life and low linear-energy-transfer [LET] radiative emissions). On the other hand, ^{211}At-astatide is also transported by NIS and offers several therapeutic advantages over ^{131}I-iodide due to its physical characteristics (short half-life, high LET α-particle emissions). The objective of this study was to directly compare the radiotoxicity of both radionuclides using a NIS-transfected cultured cell model. **Methods:** Cytotoxicity was determined by colony-forming assays. Also, a first-order pharmacokinetic model was used to simulate the closed compartmental system between the medium and cells. Experimental data were then fitted to this model and used to estimate the transfer coefficients between medium and cells, k_m^c, and between cells and medium, k_c^m. Using the pharmacokinetic model, the cumulated activity concentrations in the medium and cells were calculated. Monte Carlo transport methods were then used to assess absorbed doses from ^{131}I and ^{211}At. **Results:** ^{211}At-Astatide was significantly more cytotoxic than ^{131}I-iodide in this closed compartmental system. For ^{211}At-astatide, absorbed doses per unit administered activity were 54- to 65-fold higher than for ^{131}I-iodide. Both NIS-expressing and control cells showed increased sensitivity to ^{211}At over ^{131}I, with significantly lower D_0 (absorbed dose required to reduce the survival fraction to e^{-1}) and SF_2 (2-Gy survival fraction) values, highlighting the higher intrinsic cytotoxicity of α-particles. However, NIS-independent (nonspecific) binding of ^{211}At-astatide was higher than that of ^{131}I-iodide, therefore, yielding a lower absorbed dose ratio between NIS-transfected and -nontransfected cells. **Conclusion:** Treatment of NIS-expressing cells with ^{211}At-astatide resulted in higher absorbed doses and increased cytotoxicity per unit administered activity than that observed with ^{131}I-iodide. These results suggest that ^{211}At-astatide may be a promising treatment strategy for the therapy of NIS-expressing tumors.

J Nucl Med 2003; 44:1827–1838

Received Apr. 11, 2003; revision accepted Jul. 22, 2003.

For correspondence or reprints contact: Michael R. Zalutsky, PhD, Department of Radiology, Box 3808, Duke University Medical Center, Durham, NC 27710.

E-mail: zalut001@mc.duke.edu

It is now well established that the accumulation of iodide by the thyroid gland is mediated by the sodium/iodide symporter (NIS), an integral membrane protein expressed on the basolateral surface of the thyrocyte. Iodide is transported across the cell membrane against a concentration gradient in a sodium-dependent manner, in a process electrochemically coupled to the energy-dependent Na^+/K^+-adenosinetriphosphatase (*1*). The cloning of the NIS gene has allowed investigations into the effect of plasmid- or viral-mediated NIS expression on the iodide-concentrating capacity in a variety of thyroid and nonthyroid cell types (*2*). These studies have indicated that NIS transgene expression, under the control of a variety of promoters, confers iodide uptake capacity in a wide range of cell lines, allowing the possibility of radioiodide therapy for many tumor types. However, several of these studies also report that the efflux of iodide from NIS-transfected cells, including anaplastic thyroid cells, is extremely rapid (*3–6*). This observation is of fundamental importance for any endoradiotherapeutic strategy, as radiation-absorbed dose (and thus treatment efficacy) is a function of the cellular residence time and physical half-life ($t_{1/2}$) of the radionuclide (*7*), with optimal conditions reached when the radiologic $t_{1/2}$ matches the biologic $t_{1/2}$ (i.e., cellular retention). Dosimetric calculations and subsequent in vivo studies, using a murine xenograft model, have indicated that successful treatment of low-retention NIS-expressing tumor deposits with ^{131}I-iodide ($t_{1/2}$ = 8.04 d) may not possible without the administration of prohibitively high activities of radioiodide (*8–10*). In addition, the effectiveness of ^{131}I in curing micrometastatic disease decreases with tumor size, due to the relatively long path length of the β-particle (*11*), resulting in an increased probability of disease recurrence.

Astatine (astatide), the heaviest of the halogens, exhibits a pronounced accumulation in the thyroid gland in halide form and in the stomach (*12*). We have previously demonstrated NIS-mediated accumulation of astatide, with uptake and efflux characteristics almost identical to those of iodide (*4*). Fortunately, ^{211}At has a physical $t_{1/2}$ of 7.214 h, which

closely matches the biologic $t_{1/2}$ reported for iodide in a variety of NIS-expressing xenograft models (*9,13,14*), unlike the physical $t_{1/2}$ of ^{131}I. In addition, the decay of ^{211}At results in the emission of α-particles with a mean linear energy transfer (LET) of 97 keV/μm. This value, representing the ionizing energy deposited by the particulate emission per unit distance, is approximately 500 times that of the therapeutic β-emitting radionuclides ^{90}Y and ^{131}I. Upon interaction with DNA, this high density of ionization events result in a high incidence of generally irreparable double-strand DNA breaks, which accounts for the extreme radiotoxicity of this radionuclide (*15*). Also, the short range of ^{211}At α-particles in tissue (maximum range, 70 μm) makes such emissions more effective for the sterilization of micrometastatic tumor clusters than β-particles. Another advantage of α-particle therapy is that cell survival is independent of dose rate, which is of particular significance in relation to the rapid uptake and efflux kinetics of radiohalides in NIS-expressing cells lacking an organification mechanism.

This article describes in vitro studies directed at evaluating the hypothesized cytotoxic advantages of ^{211}At-astatide over ^{131}I-iodide for the treatment of NIS-expressing cells lacking a halide organification mechanism. Experiments were performed using the human glioma cell line UVW, transfected with human NIS complementary DNA (cDNA) (called NIS6 hereafter), using the parental cell line (UVW) as a negative control. The sensitivity of each cell line to external beam irradiation was established by clonogenic assay, allowing comparison of intrinsic radiosensitivity in both cell lines and also of the cellular sensitivity to both low and high LET particle-emitting radionuclides. Sensitivity of both cell lines to varying activity concentrations of ^{131}I-iodide and ^{211}At-astatide was also established by colony-forming assay. A pharmacokinetic model was derived to describe the closed compartmental system between the medium and cells. Experimentally derived kinetic data were then fitted to this model and used to estimate transfer coefficients between medium and cells. Using the pharmacokinetic model, the cumulated activity concentrations in the medium and cells were calculated. Monte Carlo transport methods were then used to assess absorbed doses from ^{131}I and ^{211}At, which were correlated with the radionuclide sensitivity data, allowing the determination and comparison of radiobiologic parameters for both cell lines to each irradiation modality.

MATERIALS AND METHODS

Cell Culture

The human glioma cell line UVW (European Collection of Cell Cultures no. 86022703) was transfected with cDNA encoding the human NIS gene to create the NIS6 cell line with a method that has previously been described (*4*). Cells were maintained in Eagle's minimal essential medium (Gibco), supplemented with 10% fetal bovine serum (Hyclone), penicillin/streptomycin (100 U/mL), and fungizone (2 mg/mL) (Gibco). Cells were cultured at 37°C in a 5% CO_2 atmosphere. Transfected cells were maintained in geneticin G-418 sulfate (0.5 mg/mL) (Gibco) in addition to the conditions described above.

External Beam Irradiations

Cells were trypsinised, counted, and resuspended in sterile tubes containing 5 mL fresh medium to a final concentration of 5×10^5 cells per milliliter. Irradiations (0–9 Gy) were performed using a 6-MV external photon beam accelerator at a dose rate of 0.5 Gy-min^{-1} with the appropriate bolus to ensure full buildup of the radiation beam. Cells were plated for colony-forming assay in 6-well plates (growth area, 9.6 cm^2) and grown at 37°C in a 5% CO_2 atmosphere for 7–10 d. Colonies were then stained and counted, with colonies comprising 50 or more cells scored as viable.

Radionuclides

The radionuclide ^{211}At was produced at the Duke University Medical Center CS-30 cyclotron via the ^{209}Bi(α, 2n)^{211}At reaction using the MIT-1 internal target system as previously described (*12*). ^{211}At was distilled from the molten bismuth target and trapped in a cooled condenser. It was then isolated from the condenser by washing with approximately 1 mL phosphate-buffered saline (PBS), pH 7.4. After isolation, Na_2SO_3 (Mallinckrodt) was added to a final concentration of 2×10^{-4} mol/L, to minimize the formation of higher oxidation state species. Sodium ^{131}I-iodide (no carrier added) was purchased from Dupont–New England Nuclear.

Pharmacokinetics

Experiments were carried out to assess the uptake and efflux pharmacokinetics of radiohalides. Cells were plated in 24-well plates at approximately 5×10^4 cells per well and allowed to attach overnight. For radionuclide uptake curves, cells were incubated for 1–30 min in wells with 0.5 mL PBS containing either ^{211}At-astatide (100 kBq/mL) or ^{131}I-iodide (50 kBq/mL). ^{211}At-astatide uptake and ^{131}I-iodide uptake were terminated by the removal of the radiohalide-containing incubation buffer, followed by 3 rapid washes in ice-cold PBS. Cells were then solubilized by the addition of 0.5 mL lysis buffer (0.1 mol/L NaOH, 1% sodium dodecyl sulfate, 2% Na_2CO_3) and assessed for radioactivity using an LKB 1282 γ-counter (LKB), in dual-channel mode. For radiohalide efflux studies, cells were plated as described above in PBS containing ^{211}At-astatide (100 kBq/mL) and ^{131}I-iodide (50 kBq/mL) for 30 min. Radioactive incubation buffer was then removed, and cells were incubated in PBS containing 1×10^{-3} mol/L thiocyanate ion (SCN^-) to inhibit the reuptake of radiohalide for the various time intervals to ensure the same conditions used in the colony-forming assay. Cells were then solubilized in lysis buffer and assessed for radioactivity using a γ-counter.

To assess variation in total uptake as a function of cell density (number of cells per unit volume d_c), cells were plated at various cell numbers between 1×10^4 and 5×10^5 per well and incubated as described above in 0.5 mL PBS containing either ^{211}At-astatide (100 kBq/mL) or ^{131}I-iodide (50 kBq/mL) for 30 min. Cells were then washed and counted for radioactivity with exact cell numbers determined with a hemocytometer. In this manner, we were able to estimate the uptake fraction as a function of cell density.

Cell Survival Fraction Assay

UVW and NIS6 cells were seeded in 24-well plates and allowed to attach for 24 h. Culture medium was then aspirated and replaced with fresh medium containing ^{131}I-iodide (0–5 MBq/mL) or ^{211}At-

astatide (0–50 kBq/mL). For the cell survival fraction assay, cells were incubated for 30 min at 37°C in a 5% CO_2 atmosphere. The total number of cells per well was determined by hemocytometer counting to assess the cell density d_c. Cells were then given 3 rapid washes in PBS, trypsinized, and plated for colony-forming assay as described above. After 10–14 d, colonies were stained and counted, with colonies comprising 50 or more cells scored as viable. Absorbed dose calculations were then carried out to assess the survival fraction as a function of absorbed dose and estimate the radiotoxicity of ^{211}At-astatide and ^{131}I-iodide.

Pharmacokinetic Model of Halide Distribution

Figure 1 illustrates a closed system describing the distribution of halide anion between medium and cells, and the differential equations that describe this closed system, following Michaelis–Menten kinetics, are given by:

$$\left.\begin{aligned}\frac{dn_m}{dt} &= -\frac{V_{\max}}{K_m + n_m} d_c v_c n_m + k_c^m \frac{d_c v_c}{(1 - d_c v_c)} n_c \\ \frac{dn_c}{dt} &= +\frac{V_{\max}}{K_m + n_m} d_c v_c n_m - k_c^m \frac{d_c v_c}{(1 - d_c v_c)} n_c\end{aligned}\right\}, \quad \text{Eq. 1}$$

where n_m is the average molar concentration of the nuclide in the medium; n_c is the average molar concentration in a cell (mol/L); $V_{\max}$ is the theoretic maximum transfer rate (mol/L s^{-1}); and K_m is the Michaelis–Menten constant for NIS in this system (mol/L); v_c is the average volume of an adherent cell (cm^3); $d_c = N_c/V_T$ is the cell density (cell cm^{-3}); and N_c is the total number of cells. We have previously estimated the K_m for NIS in this system as 35 μmol/L with respect to iodide (*4*) but were unable to obtain a similar estimate using astatide due to the absence of a stable astatine isotope. However, we have previously demonstrated that astatide competes equally with iodide in this system (*16*) and, therefore, assume that the K_m value for astatide is similar to that of iodide.

The maximum initial molar concentrations used in our clonogenic studies of either ^{211}At-astatide or ^{131}I-iodide in the medium (6.2×10^{-6} and 8.2×10^{-3} μmol/L, respectively) were several orders of magnitude smaller than the K_m value estimated for iodide. Consequently, when $n_m \ll K_m$, the above equations can be approximated as:

$$\left.\begin{aligned}\frac{dn_m}{dt} &= -k_m^c d_c v_c n_m + k_c^m \frac{d_c v_c}{(1 - d_c v_c)} n_c \\ \frac{dn_c}{dt} &= +k_m^c d_c v_c n_m - k_c^m \frac{d_c v_c}{(1 - d_c v_c)} n_c\end{aligned}\right\}, \quad \text{Eq. 2}$$

where $k_m^c = V_{\max}/K_m$ is the transfer constant from the medium to a cell (s^{-1}) where the net transfer rate is given by $V_{\max} d_c v_c / K_m$, and k_c^m is the transfer constant from a cell to the medium (s^{-1}); N_c is the total number of cells; and $V_c = N_c v_c$ is the volume of all cells (cm^3); $V_T = V_m + V_c$ where V_T is the total volume of the system (cm^3); and V_m is the volume of the incubation medium (cm^3). During uptake (u), the initial conditions are $n_m^0 = cte$, $n_c^u = 0$, and by conservation of mass $V_m n_m^0 = V_m n_m^u + N_c v_c n_c^u$, where $d_c^u = N_c/V_T^u$ is the cell density and V_T^u is the volume of the system during the uptake period; thus, the solutions for n_m^u and n_c^u are:

$$\left.\begin{aligned} n_m^u(t) &= \frac{n_m^0}{(d_c^u v_c k_m^c + k_c^m)} \left[(d_c^u v_c k_m^c) e^{-(k_m^c v_c d_c^u + k_c^m)t} + k_c^m\right] \\ n_c^u(t) &= n_m^0 \frac{(1 - d_c^u v_c) k_m^c}{(d_c^u v_c k_m^c + k_c^m)} \left[1 - e^{-(k_m^c v_c d_c^u + k_c^m)t}\right]\end{aligned}\right\}, \quad \text{Eq. 3}$$

where the decay-corrected fractional cell uptake $F(d_c)$ as a function of cell density d_c for an incubation period t_u is given by:

$$F(d_c) = \frac{N_c v_c n_c^u(t_u)}{V_m n_m^0} = \frac{d_c^u v_c k_m^c}{(d_c^u v_c k_m^c + k_c^m)} \left[1 - e^{-(k_m^c v_c d_c^u + k_c^m)t_u}\right], \quad \text{Eq. 4}$$

which tends to equilibrium conditions when $t \to \infty$; thus, $F(d_c) \to d_c v_c k_m^c / (d_c v_c k_m^c + k_c^m)$. This expression is used to estimate the values of k_m^c and k_c^m by means of nonlinear regression analysis from experimental observations. The solutions during efflux (e) for n_m^e and n_c^e after an incubation period t_u and removal of the medium and dilution to a new cell density $d_c^e = N_c/V_T^e$ are:

$$\left.\begin{aligned} n_m^e(t) &= \frac{d_c^e v_c n_c^0}{(1 - d_c^e v_c)} \frac{k_c^m}{(d_c^e v_c k_m^c + k_c^m)} \left[1 - e^{-(k_m^c d_c^e v_c + k_c^m)(t - t_u)}\right] \\ n_c^e(t) &= \frac{n_c^0}{(k_m^c d_c^e v_c + k_c^m)} \left[k_c^m e^{-(k_m^c d_c^e v_c + k_c^m)(t - t_u)} + k_m^c d_c^e v_c\right]\end{aligned}\right\}, \quad \text{Eq. 5}$$

where V_T^e is the total volume of system during efflux; $n_c^0 = n_c^u(t_u)$ is the initial molar concentration of cells; and by conservation of mass $N_c v_c n_c^0 = V_m n_m^e + N_c v_c n_c^e$ any time afterwards. The activity concentration in the medium a_m and in cells a_c are then given as:

$$\left.\begin{aligned} a_m(t) &= 1 \times 10^{-3} \lambda N_A \rho_m^{-1} e^{-\lambda t} \begin{cases} n_m^u(t) & 0 \le t \le t_u \\ n_m^e(t) & t > t_u \end{cases} \\ a_c(t) &= 1 \times 10^{-3} \lambda N_A \rho_c^{-1} e^{-\lambda t} \begin{cases} n_c^u(t) & 0 \le t \le t_u \\ n_c^e(t) & t > t_u \end{cases}\end{aligned}\right\}, \quad \text{Eq. 6}$$

where N_A is Avogadro's number; ρ_m and ρ_c are the densities of the medium and cells, respectively; and λ is the physical decay constant for the radionuclide in consideration. The cumulated activity concentration in the medium $\tilde{a}_m$ and in the cells $\tilde{a}_c$ are then given as:

$$\left.\begin{aligned} \tilde{a}_m &= \tilde{a}_m^u + \tilde{a}_m^e \\ \tilde{a}_c &= \tilde{a}_c^u + \tilde{a}_c^e\end{aligned}\right\}, \quad \text{Eq. 7}$$

where $\tilde{a}_m^u$ and $\tilde{a}_c^u$ are the cumulated activity concentration in the medium and a cell during uptake, respectively; and $\tilde{a}_m^e$ and $\tilde{a}_c^e$ are the corresponding cumulated activity concentrations for the medium and cells during efflux, respectively. The expressions for $\tilde{a}_m^u$, $\tilde{a}_m^e$, $\tilde{a}_c^u$, and $\tilde{a}_c^e$ are given in Appendix A. The total cumulated activity per cell is then given as:

$$\tilde{q}_c = v_c(\tilde{a}_c^u + \tilde{a}_c^e), \quad \text{Eq. 8}$$

where v_c is the average volume of a cell. Because this compartmental model is a closed system, the residence time of the radionuclide in the medium and cells during uptake is given by $\tau^u = \tau_m^u + \tau_c^u = \lambda^{-1}(1 - e^{-\lambda t_u})$, and during efflux as $\tau^e = \tau_m^e + \tau_c^e = \lambda^{-1} d_c v_c (1 - d_c v_c)^{-1} a_c^0 / a_m^0$, where a_c^0 is the cell activity concentra-

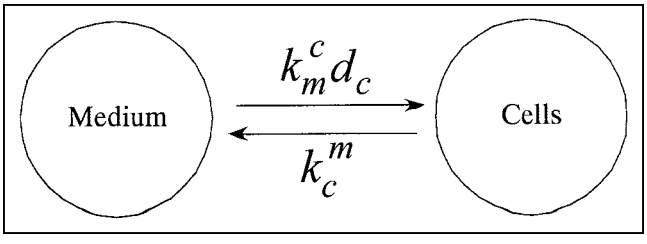

FIGURE 1. Compartmental model describing distribution of NIS substrate anions between medium and cell.

tion after an incubation period t_u. A glossary of the terminology used is given in Appendix B.

Small-Scale Dosimetry of ^{131}I-Iodide

Dosimetry of ^{131}I-iodide was carried out using the EGS4 Monte Carlo transport code, which was estimated using the geometry utilized in the in vitro assays (*17–19*). The cell nucleus was considered to be the target in these calculations. UVW and NIS6 cells were stained using Cyto16 (Molecular Probes), which binds to nucleic acids. Phase-contrast and fluorescent images of cells were obtained and superimposed and used as a model for these calculations (Fig. 2). In these dosimetric calculations, 2 sources were identified: the medium where the activity was diluted, and the attached cells themselves, which take up the activity from the medium. The images provided the basic cell morphology that was used in these calculations. The nucleus of adherent cells had a semiellipsoid geometry. However, for simplification purposes, we used a spheric model of the cell and nucleus, where the volume of the semiellipsoid nucleus was that of the sphere nucleus. Thus, the estimated average cell and nuclear diameter used in these studies were 16 and 10 μm, respectively.

The estimated dose conversion factor for ^{131}I-iodide when the source was the medium and the target was the cells, $S(m \rightarrow c)$, was 1.48×10^{-11} Gy g Bq^{-1} s^{-1}, and the dose conversion factor when both the source and the target were the cells, $S(c \rightarrow c)$, was 5.5×10^{-4} Gy Bq^{-1} s^{-1}. These dose conversion factors were used to assess the total absorbed dose to UVW and NIS6 cells from ^{131}I-iodide. The total average absorbed dose to a cell is then given as:

$$D = \tilde{a}_m S(m \rightarrow c) + \tilde{q}_c S(c \rightarrow c), \qquad \text{Eq. 9}$$

where $\tilde{a}_m$ is the cumulated activity concentration in the medium and $\tilde{q}_c$ is the average cumulated activity in a cell (Bq s).

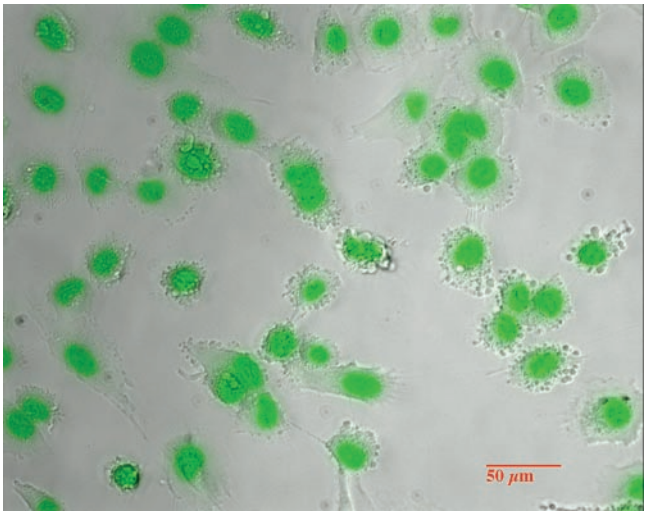

FIGURE 2. Superimposition of phase-contrast and fluorescent images of adherent cells labeled with Cyto16 nuclear stain to show nuclear and cell morphology of UVW and NIS6 cell lines. Colony-forming assays were performed under similar conditions. Images were used to derive cellular and nuclear geometry, which subsequently was used in calculations to determine cumulated absorbed dose. Strongly green regions identify cell nuclei.

Microdosimetry of ^{211}At-Astatide

Microdosimetry of ^{211}At-astatide was carried out using an α-particle Monte Carlo transport code as described elsewhere (*20*). The cell nucleus was considered to be the target in these calculations. The total absorbed dose is then given as:

$$D = \tilde{a}_m h_m^c \bar{z}_{1m}^c + \tilde{q}_c h_c^c \bar{z}_{1c}^c, \qquad \text{Eq. 10}$$

where D is average absorbed dose (Gy); $\tilde{a}_m$ is the total cumulated activity in the medium (Bq s g^{-1}); h_m^c is the average number of hits from medium to cells (hits g Bq^{-1} s^{-1}); $\bar{z}_{1m}^c$ is the average specific energy per event from medium to cells (Gy hit^{-1}); $\tilde{q}_c$ is the cumulated activity per cell (Bq s cell^{-1}); h_c^c is the average number of hits from cells to cells (hits Bq^{-1} s^{-1}); and $\bar{z}_{1c}^c$ is the average specific energy per event from cells to cells (Gy hit^{-1}). The values for h_m^c, h_c^c, $\bar{z}_{1m}^c$, and $\bar{z}_{1c}^c$ were estimated as a function of cells per unit area to account for cross fire among cells (data not shown). As an example, a cylindric well (diameter, 16.5 mm) containing 1.4×10^5 adherent cells resulted in a surface cell density of 655 cells mm^{-2}, and the corresponding conversion factors for $\bar{z}_{1m}^c$, $\bar{z}_{1c}^c$, h_m^c, and h_c^c were 0.224 Gy hit^{-1}, 0.114 Gy hit^{-1}, 4.456×10^{-9} hit cm^3 Bq^{-1} s^{-1}, and 0.407 hit Bq^{-1} s^{-1}, respectively.

RESULTS

External Beam Radiation

Data obtained from the external beam radiation dose/survival assay were fitted using the linear quadratic model of cell survival $SF = \exp(-\alpha D - \beta D^2)$, where SF is the surviving fraction and D is the absorbed dose (Fig. 3). Using the statistical analysis software SAS, we carried out the model fitting to assess the parameters α and β. The estimated 2-Gy survival fraction, SF_2, for UVW and NIS6 cell lines was 0.71 (0.62–0.83, 95% confidence interval [CI]) and 0.61 (0.53–0.70, 95% CI), respectively. There was no statistically significant difference for the SF_2 between the 2 cell lines based on a t test with equal variances ($P = 0.3$) (SAS).

Radionuclide Uptake and Efflux Pharmacokinetics

The decay-corrected fraction of administered activity taken up by the cells after a 30-min incubation period $F(d_c)$ was estimated as a function of cell density d_c for ^{211}At-astatide and ^{131}I-iodide for UVW and NIS6 cell lines. Figure 4 shows the experimental data for NIS6 and UVW cell lines illustrating both specific and nonspecific cellular uptake. The uptake of ^{131}I-iodide and ^{211}At-astatide by NIS6 cells was approximately 60- and 27-fold higher than that of the nontransfected UVW (control), respectively. Also, the nonspecific (NIS independent) association of ^{211}At-astatide was about 4-fold higher that that of ^{131}I-iodide, possibly due to the presence of a higher oxidation state of astatine in the aqueous solution (*16*). Using nonlinear regression analysis, the transfer coefficients k_m^c and k_c^m were derived based on the observed efflux kinetics (Fig. 4A) and the expression for $F(d_c)$ (Fig. 4B). Table 1 shows the estimated values for k_m^c and k_c^m for UVW and NIS6 cell lines. In each instance, k_m^c was higher than k_c^m, indicating that, in the presence of an extracellular halide ion concentration, there is a net associ-

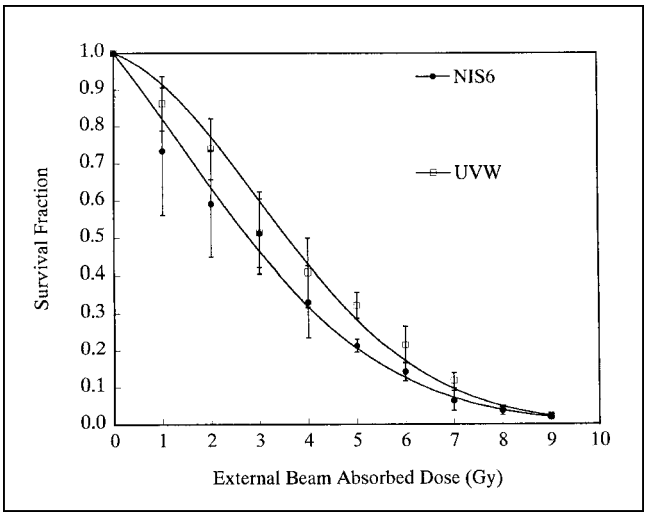

FIGURE 3. Survival fraction of NIS6 and UVW as function of external beam radiation-absorbed dose. Points represent average of triplicate determinations and corresponding SD. External beam dose rate was 0.5 Gy min^{-1}. The estimated 2-Gy *SF* (95% confidence interval [CI]) was 0.71 (0.62–0.83, 95% CI) and 0.61 (0.53–0.70, 95% CI) for UVW and NIS6, respectively. There was no statistically significant difference between NIS6 and UVW cells lines ($P = 0.296$).

ation of ion with the cell. The net rate of accumulation of astatide and iodide by NIS6 cells was 32.5- and 27.2-fold higher than that observed for UVW cells, respectively. We observed that astatide had a higher k_m^c and lower k_c^m value than iodide with respect to UVW cells, reflecting the higher nonspecific association of astatide previously reported (*16*).

Pharmacokinetic Model of Halide Distribution

This model describes the distribution of ^{131}I-iodide and ^{211}At-astatide between the incubation medium and cells over time in the presence (uptake) and absence (efflux) of halide anions. For the purposes of these studies, we modeled a closed system to reproduce the incubation conditions used in the colony-forming assays. The uptake and efflux rate constants of the system (k_m^c and k_c^m, respectively) were determined from the experimental data as described above. Figure 5 is a representative example of the pharmacokinetics of ^{211}At-astatide in NIS6 and UVW cells during uptake and efflux phases. This system is sensitive to cell density in the assay system (d_c), as highlighted in Fig. 5B. During the efflux phase, the system reequilibrates as ^{211}At-astatide moves from cells to medium and is then subject to reuptake (upper curve). Reduction of the cell density during the efflux phase, as occurs during plating for colony-forming assay, results in equilibration at a much lower cellular concentration (lower curve). This effect is more pronounced in NIS6 cells (Fig. 5B) than in UVW cells (Fig. 5A), as the total nonspecific cell-associated activity is many fold lower than NIS-mediated uptake.

Administered Activity Concentration Versus Survival Fraction

The effect of increasing radionuclide concentration on clonogenic survival was assessed in UVW and NIS6 cells using both ^{131}I-iodide and ^{211}At-astatide. An activity concentration-dependent decrease in surviving clonogens was observed after treatment of NIS6 cells with both radionuclides (Fig. 6). For both radionuclides examined, the control parental UVW cell line was less sensitive than the NIS-transfected cell line, indicating the preferential therapeutic efficacy in NIS-expressing cells over control cells.

The survival data were fitted using a single exponential and, for the purpose of comparison, we used this model to calculate A_0, which indicates the initial activity concentra-

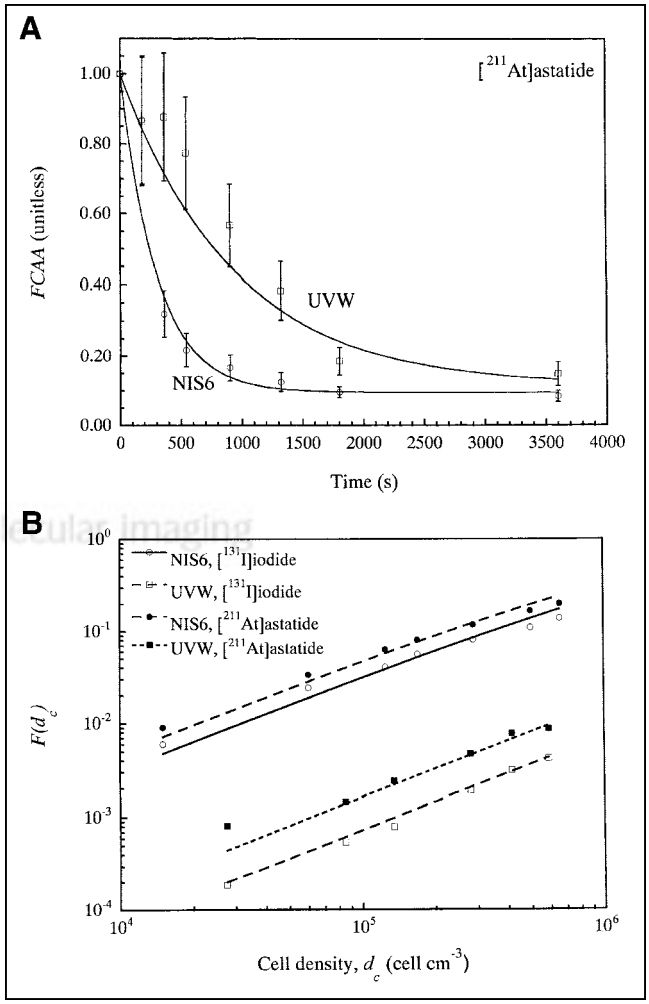

FIGURE 4. (A) Fractional cell-associated activity (*FCAA*) of ^{211}At-astatide for UVW and NIS6 cell lines during efflux as function of time. Similar curves were generated using ^{131}I-iodide (data not shown). Data represent means ± SD from at least 2 triplicate determinations. (B) Fractional cell uptake $F(d_c)$ as function of cell density for NIS6 and UVW cell lines for incubation period of 30 min for ^{131}I-iodide and ^{211}At-astatide. Data represent means of 3 determinations. Experimental data were fitted to theoretic expression for $F(d_c)$ to estimate transfer constants k_m^c and k_c^m shown in Table 1. Uptake of ^{131}I-iodide by NIS6 cells was approximately 60-fold higher than that of UVW (nonspecific binding). Total uptake of ^{211}At-astatide to NIS6 cells was approximately 27-fold higher than that of UVW. Nonspecific binding of ^{211}At-astatide was approximately 4-fold higher than that of ^{131}I-iodide.

TABLE 1
Estimated Pharmacokinetic Parameters for ^{131}I-Iodide and ^{211}At-Astatide for UVW and NIS6 Cell Lines

	^{131}I-Iodide			^{211}At-Astatide		
	k_m^c (s^{-1})	k_c^m (s^{-1})	k_m^c/k_c^m	k_m^c (s^{-1})	k_c^m (s^{-1})	k_m^c/k_c^m
NIS6	1.96×10^{-1}	1.19×10^{-3}	164.7	4.79×10^{-1}	2.10×10^{-3}	228.1
UVW	7.20×10^{-3}	2.07×10^{-3}	3.5	1.47×10^{-2}	1.88×10^{-3}	7.8
NIS6/UVW	27.22	0.57		32.50	1.12	

k_m^c = transfer coefficient from media to cells; k_c^m = transfer coefficient from cells to media.

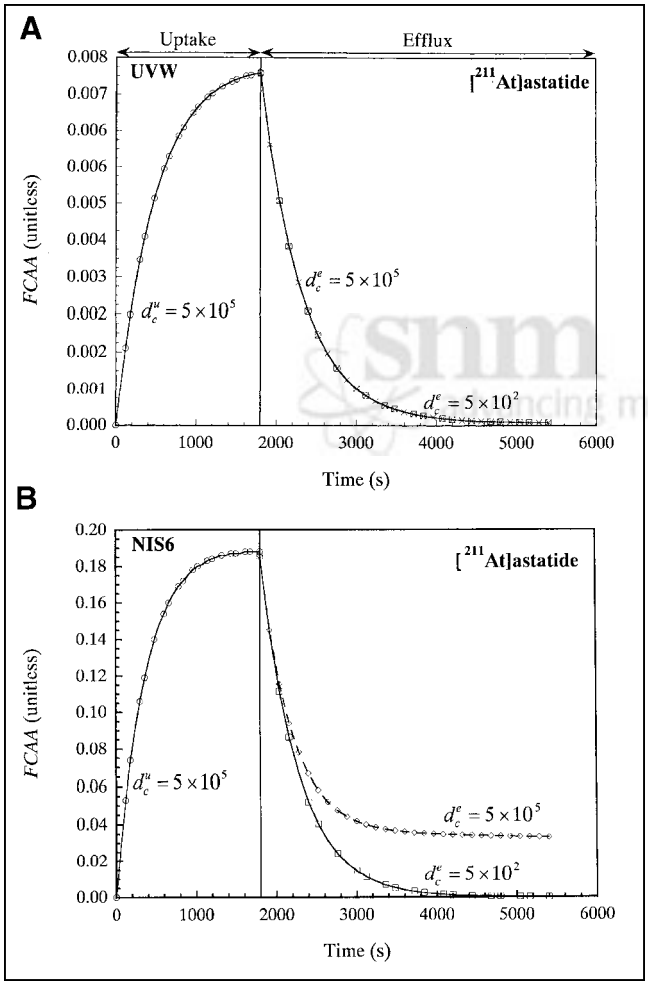

FIGURE 5. Calculated fractional cell-associated activity for UVW and NIS6 cell lines for ^{211}At. Cell density during uptake was 5×10^5. Cell density during efflux was reduced by factor of 1×10^3 cells cm^{-3}, reflecting conditions used during colony-forming assay. However, when cell density was left constant, a different efflux profile is observed as indicated in Equation 5. Uptake period was 30 min. Calculations were based upon estimated k_m^c and k_c^m coefficients that were derived from our experimental studies (Table 1). Area under the curve was calculated to assess cumulated activity concentration in cells and corresponding absorbed dose.

tions of each radionuclide required to reduce the clonogenic capacity of UVW and NIS6 cells by 1 natural logarithm (e^{-1}). These values are shown in Table 2. The A_0 ratio between UVW and NIS6 cells was 13.2-fold for ^{131}I-iodide and 11.5-fold for ^{211}At-astatide. The similarity of these values is consistent with the similar pharmacokinetics for

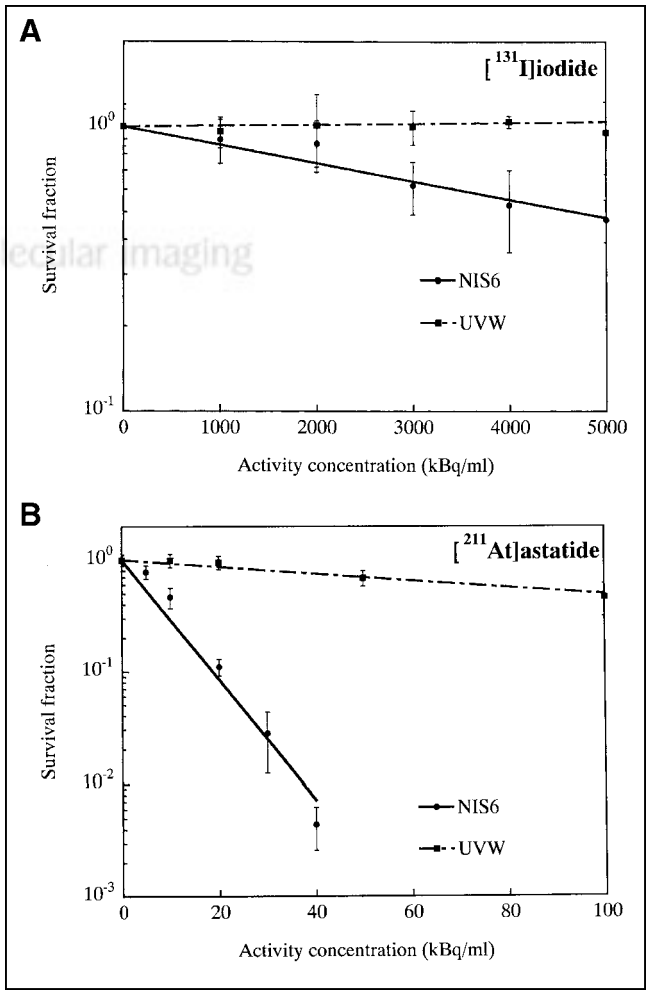

FIGURE 6. Survival fraction as function of activity concentration in medium for incubation period of 30 min. Survival fraction of NIS6 and UVW for ^{131}I (A) and for ^{211}At (B), respectively. Data represent means ± SD of at least 3 triplicate determinations. Therapeutic efficiency and toxicity ratios are given in Table 2.

TABLE 2
Effect of ^{131}I-Iodide and ^{211}At-Astatide Administration on Clonogenic Survival of UVW and NIS6 Cell Lines

	A_0 ^{131}I (MBq mL^{-1})	A_0 ^{211}At (MBq mL^{-1})	[^{131}I]/[^{211}At]
UVW	86.43	0.126	686
NIS	6.55	0.011	598
UVW / NIS6	13.2	11.5	

both radionuclides in this system. Comparison of the relative toxicity of each radionuclide (A_0 for ^{131}I divided by A_0 for ^{211}At) indicates that, in terms of radioactive concentration, ^{211}At-astatide is between 600 and 700 times more radiotoxic that ^{131}I-iodide in this model (Table 2). The higher nonspecific association of ^{211}At-astatide in this system may account for the variation observed in both of these ratios. The cumulated activity concentrations in the medium and cells were estimated by integrating the uptake-efflux kinetics over time as a function of cell density d_c and then were used to calculate the absorbed doses for UVW and NIS6 per unit administered activity (Table 3).

Correlation of Survival Fraction and Absorbed Dose

Radionuclide sensitivity data from these experiments were correlated with estimates of absorbed dose. The cumulated activity concentrations were calculated by determining the area under the curve (AUC) derived from the pharmacokinetic model. Absorbed doses were estimated by calculating the cumulated activity concentration in the medium and cells and using the corresponding conversion factors as described in Equations 9 and 10 for ^{131}I-iodide and ^{211}At-astatide, respectively. These data, shown in Figure 7, demonstrate that both UVW and NIS6 cells have a greater sensitivity to an equivalent absorbed dose of high LET α-particles (Fig. 7A) than to low LET β-particles (Fig. 7B).

Single-exponential equations were fitted to these data and fitted coefficients were used to derive D_0 and 2-Gy surviving fractions (SF_2) for each cell line and radionuclide. These data are shown in Table 4. This similarity of D_0 and SF_2 values between NIS6 and UVW using each treatment modality cells confirms that plasmid-mediated NIS expression does not alter the intrinsic cellular radiosensitivity in this model system. The SF_2 values obtained from external beam

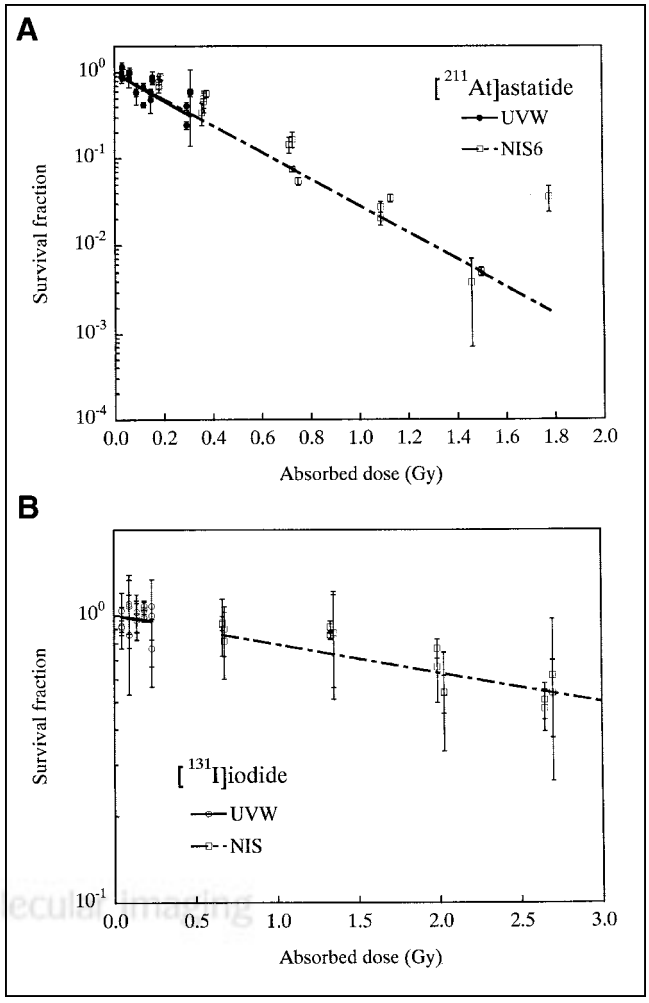

FIGURE 7. Survival fraction of UVW and NIS6 cell lines as function of absorbed dose from ^{211}At-astatide (A) and ^{131}I-iodide (B). Estimated D_0 of UVW and NIS6 for ^{211}At-astatide was 0.27 (0.19–0.46, 95% CI) Gy and 0.28 (0.26–0.30, 95% CI) Gy, respectively. 2-Gy *SF* was 6.3×10^{-4} ($3.1 \times 10^{-5} - 1.3 \times 10^{-2}$, 95% CI) and 7.4×10^{-4} ($4.2 \times 10^{-4} - 1.3 \times 10^{-3}$, 95% CI), respectively. D_0 of UVW and NIS6 for ^{131}I-iodide was 5.27 (2.5–6.4, 95% CI) Gy and 4.31 (3.0–7.6, 95% CI) Gy, respectively, and 2-Gy *SF* for UVW and NIS6 was 0.68 (0.02–20.4, 95% CI) and 0.66 (0.35–1.22, 95% CI), respectively.

TABLE 3
Average Absorbed Dose per Unit Administered Activity In Vitro of ^{131}I-Iodide and ^{211}At-Astatide in UVW and NIS6 Cells Lines

	^{131}I (Gy-mL/MBq)	^{211}At (Gy-mL/MBq)	[^{211}At]/[^{131}I]
UVW	4.59×10^{-2}	3.01	65.5
NIS	6.64×10^{-1}	36.5	55.0
NIS6 / UVW	14.5	12.0	

TABLE 4
Dose Factors and 2-Gy Survival Fraction Associated with ^{131}I-Iodide, ^{211}At-Astatide, and External Beam Radiation in UVW and NIS6 Cells Lines

	^{131}I		^{211}At		XRT
	D_0 (Gy)	SF_2	D_0 (Gy)	SF_2	SF_2
UVW	5.27	0.68	0.27	6.3×10^{-4}	0.71
NIS6	4.31	0.66	0.28	7.4×10^{-4}	0.61

XRT = external beam radiotherapy.

radiotherapy (Fig. 3) are similar to those derived from ^{131}I-iodide treatment, which is in concordance with many previous observations. However, the SF_2 values derived from ^{211}At-astatide treatment were 900- to 1,100-fold higher (Table 4) than those from both external beam radiotherapy and ^{131}I in both cell lines, reflecting the cytotoxicity of ^{211}At-astatide observed in this system (Table 2). Comparison of D_0 values for ^{211}At-astatide and ^{131}I-iodide demonstrates a 15.3- and 19.5-fold differential for UVW and NIS6, respectively, highlighting the therapeutic advantage, in terms of radiation quality, of high LET ^{211}At α-particles over low LET ^{131}I β-particles.

DISCUSSION

The transgene-mediated expression of the NIS has been demonstrated to confer iodide uptake capacity to a wide range of cell types that would not normally concentrate iodide (*2–4*). NIS gene transfer, followed by radioiodide administration, allows the possibility of treatment of tumors at many sites in a manner analogous to the highly efficacious treatment of differentiated thyroid carcinoma with radioiodide. However, the short retention time of iodide observed in nonthyroid xenografts, combined with the relatively long physical $t_{1/2}$ of ^{131}I, results in an insufficient absorbed dose for successful tumor eradication. The use of radionuclides with similar chemical properties and more favorable physical properties, such as a higher LET and shorter physical $t_{1/2}$, should result in an increased radiation dose and thus enhanced efficacy.

We have previously reported that plasmid-mediated cellular expression of the NIS confers the ability to accumulate ^{211}At-astatide in addition to iodide (*16*). Here we describe clonogenic survival experiments designed to directly compare the radiotoxicity of ^{131}I-iodide and ^{211}At-astatide on a cultured cell model and a pharmacokinetic model, which was used to estimate absorbed dose for each radionuclide in UVW and NIS6 cell lines. To determine whether expression of the NIS protein, or selection of NIS-positive clones, resulted in an alteration of cellular radiosensitivity, a comparison of the radiation sensitivity of UVW and NIS6 cell lines was performed by examining the clonogenic survival of both cell lines in response to external photon beam irradiation. The SF_2 values obtained for both cell lines were not significantly different, 0.71 (0.62–0.83, 95% CI) and 0.61 (0.53–0.70, 95% CI) for UVW and NIS6, respectively (Fig. 3), indicating that expression of NIS has no effect on intrinsic radiosensitivity. The effect of activity concentration of both ^{131}I-iodide and ^{211}At-astatide on UVW and NIS6 cells was determined by colony-forming assay. An activity concentration-dependent decrease in clonogenic survival was observed in both cell lines with both radionuclides (Fig. 6), with NIS6 cells having increased sensitivity to each radionuclide when compared with control UVW cells. Using these data, values were calculated to indicate the activity concentration required to cause a reduction in survival by 1 natural logarithm (A_0), using the incubation conditions described above. The ratio of A_0 values between NIS-negative (UVW) and NIS-expressing (NIS6) cells (ratio 1, Table 2) was 13.2 for ^{131}I-iodide and 11.5 for ^{211}At-astatide (Table 2). The similarity of these values reflects the similar pharmacokinetics of cellular iodide and astatide association in this model system. The smaller therapeutic differential calculated for ^{211}At may reflect the higher degree of nonspecific binding observed with aqueous astatide solutions (*16*,*21*). For this study, we define the terms "specific binding" as NIS-mediated, perchlorate-sensitive cellular uptake and "nonspecific binding" as non-NIS-mediated, perchlorate-insensitive cellular uptake of radiohalide. Detailed examination of the properties of specific and nonspecific uptake of both ^{131}I-iodide and ^{211}At-astatide in this model system have previously been reported (*16*). Comparison of A_0 values for each radionuclide indicated an enhanced sensitivity to ^{211}At of 686-fold in UVW cells and 598-fold in NIS6 cells compared with ^{131}I. Similar enhancements in sensitivity (up to 1,400-fold) were observed previously when comparing the cytotoxicity of ^{211}At- and ^{131}I-labeled benzylguanidine compounds in neuroblastoma cells (*22*). These data, and our own observations, are in accordance with calculations that predict a 1,200-fold increase in cytotoxicity for α-particles on a single cell basis (*23*). It should be noted that A_0 values, expressed in units of activity per unit volume (Bq mL^{-1}) only indicate the relative toxicity of each radionuclide under the experimental conditions used for these studies. Calculation of cumulated absorbed dose from each radionuclide also requires that radiologic $t_{1/2}$ and system geometry be taken into account. Absorbed dose calculations indicate that administration of ^{211}At-astatide results in an increase (53.9- to 64.9-fold) over ^{131}I-iodide in absorbed dose per administered activity concentration (Table 3).

The rapid efflux of iodide from NIS-expressing cells lacking an organification mechanism has been observed in several cell lines and rodent xenograft models (*4*,*9*,*24*). The biologic $t_{1/2}$ of iodide in xenograft tumors is generally longer than that observed in 2-dimensional cultured cell models, presumably due to the continual reuptake of iodide by the tumor. Although this has allowed effective demonstrations of the potential of NIS expression for tumor imaging using NIS substrate molecules such as $^{123}I^-$, $^{124}I^-$, and $^{99m}TcO_4^-$ (*25–27*), the successful sterilization of such tumors with ^{131}I is likely to require the administration of prohibitively large quantities of radioactivity (*9*). However, studies performed using an in vivo prostate model have demonstrated, given sufficiently high administered radioactivity, that nonthyroid tumor xenografts with transgene-mediated NIS expression can be successfully treated with ^{131}I (*8*). This demonstrates the principle that NIS-expressing tumor deposits can be successfully targeted and treated with an ionic radiohalide in vivo and that the therapeutic effect is dependent on delivering a sufficient radiation dose to tumor.

α-Particle-emitting radionuclides have considerable potential as cytotoxic agents in the treatment of malignant disease. The short range and high LET α-particle makes their use particularly suited to the treatment of micrometa-

static and minimal residual disease, where the radiation dose to tumor is normally limited by the dose delivered to surrounding normal tissues. Tumor-specific targeting of α-particles can result in highly focal irradiation, high tumor absorbed doses, and minimization of surrounding normal tissue toxicity. The first clinical trial with an ^{211}At-labeled therapeutic antibody (antitenascin monoclonal antibody 81C6) is currently underway, with encouraging initial observations of high radiation doses to the target area and low doses to surrounding normal tissue (*28*).

The data presented in this article indicate that the administration of ^{211}At-astatide results in a significant increase (55- to 65.6-fold) over ^{131}I-iodide in absorbed dose per administered activity concentration (Table 3). However, the nonspecific association of ^{211}At-astatide with cells lacking NIS expression also contributes to the dose to these cells, resulting in a lower therapeutic differential than that observed with ^{131}I-iodide at the same administered activity concentration (12.0 and 14.5, respectively) (Table 3).

A previous study evaluating the uptake of ^{211}At-astatide by NIS transgene-expressing thyroid tumor cells (*21*) presented several observations similar to our current and previously published data (*16*). Uptake and efflux kinetics of both ^{211}At-astatide and ^{131}I-iodide are similar in each cultured cell model system, and uptake of both radiohalides was sensitive to excess perchlorate (ClO_4^-) and iodide (I^-) concentration, demonstrating that ^{211}At-astatide is transported by NIS with an efficiency approaching that of iodide. Using a murine xenograft model, the intraperitoneal administration of ^{211}At-astatide resulted in a 14.4-fold increase in tumor absorbed dose over that predicted for ^{131}I-iodide, with similar biologic half-lives observed for both anions (*21*). Although the difference in pharmacokinetics between in vitro and in vivo models precludes a direct comparison of absorbed dose, the conclusions of Petrich et al. (*21*), in accordance with this study, indicate that the administration of ^{211}At-astatide results in a significantly higher absorbed dose to NIS-expressing cells than ^{131}I-iodide per unit administered activity.

The pharmacokinetic model presented in this study describes the phenomenologic distribution of halide anions in a closed system, which accurately describes the conditions used in the cultured cell clonogenic assays described above. It is also possible to use this model to analyze the pharmacokinetics of other NIS substrate anions, such as $^{188}ReO_4^-$ or $^{99m}TcO_4^-$, under similar experimental conditions. In addition, it can also be adapted, given appropriate experimental observations, to predict the effect of alteration of many system parameters (e.g., level of NIS expression, heterogeneous cell populations, pharmacologic inhibitors of halide efflux) on both pharmacokinetic distribution and cumulated absorbed dose. We intend to further develop this model to examine the pharmacokinetics of NIS-mediated anion transport in a 3-dimensional cultured cell system and, in combination with biodistribution data, to develop a model describing the pharmacokinetics in a dynamic extracellular system similar to that encountered in vivo, which will aid in the future design of NIS-based therapeutic strategies.

Given the similar pharmacokinetics of ^{131}I-iodide and ^{211}At-astatide in our model system, our observation of a higher absorbed dose using ^{211}At-astatide can be explained by a combination of the higher energy α-particle (5.87 MeV) versus ^{131}I β-particle emission (0.6 MeV) as well as the shorter physical $t_{1/2}$ of ^{211}At (7.2 h vs. 192 h for ^{131}I). Similarly, a study into the potential of ^{188}Re (in the form $^{188}ReO_4^-$) to sterilize NIS-expressing cells calculated a 4.5-fold higher absorbed dose, when compared with ^{131}I (*14*). This enhancement is likely due to a combination of factors: ^{188}Re emits β-particles with a higher energy than ^{131}I (2.12 vs. 0.61 MeV), and ReO_4^- had higher tumor uptake than I^- in a NIS-expressing xenograft model (*14*). However, much of the increase in absorbed dose results from the comparatively short physical $t_{1/2}$ (16.7 h) of ^{188}Re (*14*). These findings are of particular significance in relation to cell types lacking a peroxidase-based organification mechanism, as these cells generally exhibit a very short cellular retention of iodide (*3,4*), and matching of both the physical and biologic half-lives of the radioisotope is desirable for maximal radiobiologic effect.

In vivo, tumor cells may show a heterogeneous expression of NIS that can be predicted to result in a heterogeneous cumulated activity distribution with the tumor mass. However, depending on the range of the radiations emitted by the radionuclide used for therapy, there is a potential for cross fire among tumors cells. Although the range of α-particles is significantly shorter than that of β-particles, a degree of cross fire can be predicted. The proportion of cells receiving a highly toxic absorbed dose from ^{211}At-astatide will therefore depend on a combination of the overall transfection efficiency, the spatial distribution of transgene expression and radionuclide within the tumor, and the degree of cross fire. The use of cultured cell models, such as the one described here, affords the opportunity for detailed analysis of these issues and may provide the basis for a clinical implementation of transgene-mediated radionuclide therapy in the future. It is also important to note that there are some tumor types, such as thyroid and invasive breast carcinoma, that may express sufficient NIS to facilitate ^{211}At-astatide therapy without the need for transgene-mediated expression.

The use of ionic ^{211}At-astatide for the treatment of thyroid carcinoma has previously been investigated in murine xenograft models, with high tumor uptakes reported for more differentiated thyroid tumor cells, which generally retain a higher level of NIS expression than anaplastic thyroid tumors (*29–31*). A study comparing the uptake of ^{125}I-iodide and ^{211}At-astatide in nude mice bearing human fetal thyroid and human malignant thyroid xenografts observed that the human tissue accumulated both halides with similar kinetics, suggesting that ^{211}At-astatide may be an alternative radionuclide to ^{131}I-iodide for the treatment of thyroid carcinoma (*29*). Another study examining the comparative

transport of ^{125}I-iodide and ^{211}At-astatide using normal porcine thyrocytes in a polarized system also observed similarities in the basal membrane (i.e., NIS mediated) transport of both radiohalide anions (*32*). Interestingly, this study also reported the perchlorate- and ouabain-insensitive basal membrane transport of astatide, by normal thyrocytes, suggesting the possibility of another, NIS-independent astatide uptake mechanism in these cells. Further elucidation of this transport mechanism may provide some explanation as to the differences in biodistribution of astatide and iodide, in addition to providing another means of targeting astatine to tumor cells.

The biodistribution of systemically administered ^{211}At-astatide, though similar to that of iodide, has several clinically relevant differences. In particular, a significantly higher uptake than iodide in both lung and spleen tissues is observed (*12*,*33*). At present, clinical trials of ^{211}At-astatide for the treatment of thyroid carcinoma have not been initiated, possibly because of concerns over radiotoxicity in these tissues or due to the limited availability of the radionuclide. Previous investigations have revealed that pharmacologic intervention may modify the level of astatide uptake in normal tissues (*12*), and further studies into the possible mechanisms involved in the lung and spleen retention of astatide are currently underway. Although lung and spleen uptake currently precludes the systemic administration of ^{211}At-astatide, combined gene transfer/radionuclide treatment of compartmentalized tumors such as those of brain, bladder, and ovary may be possible with minimal involvement of the systemic circulation. Further advances in the understanding of the mechanisms of astatine uptake and retention in lung and spleen will aid greatly in the clinical implementation of systemic ^{211}At-astatide therapy for tumors with both endogenous and gene transfer–mediated NIS expression.

CONCLUSION

The data presented in this article demonstrate that ^{211}At-astatide has potential as an alternative radionuclide to ^{131}I-iodide for the treatment of NIS-expressing tumor cells. The direct comparison of ^{211}At and ^{131}I in this closed system highlights the enhancements in absorbed dose and radiotoxicity of high LET α-particles over low LET β-particle irradiation. ^{211}At-Astatide administration results in increased cytotoxicity (686- to 598-fold) and higher absorbed doses (55- to 65.5-fold) per unit administered activity when compared with ^{131}I-iodide. In addition, the physical $t_{1/2}$ of ^{211}At is closely matched to the radionuclide residence time observed in nonthyroid tumor types, providing a further therapeutic advantage over ^{131}I. These observations imply that some of the limitations of ^{131}I administration for the therapy of endogenous or transgene-mediated NIS-expressing tumors can be overcome. The pharmacokinetic model presented here is a valuable tool in predicting the influence on absorbed dose resulting from modulation of many experimental system parameters. Further development of this model to describe a 3-dimensional tumor within a dynamic environment will aid in the elucidation of the relationship between administered radioactivity and resulting absorbed doses in NIS-expressing tumors with different retention characteristics.

ACKNOWLEDGMENTS

NIS cDNA was kindly provided by Dr. Sissy M. Jhiang (Ohio State University, Columbus, OH). This work was supported by grants CA42324, CA70164, and CA91927 from the National Institutes of Health and by an AstraZeneca Union Internationale Contre le Cancer Translational Cancer Research Fellowship (American Cancer Society Beginning Investigator 11/2001).

APPENDIX A

Pharmacokinetics

System description:

$$\frac{dn_m}{dt} = -k_m^c d_c v_c n_m + k_c^m \frac{d_c v_c}{(1 - d_c v_c)} \qquad n_c, \frac{dn_c}{dt} = +k_m^c d_c n_m - k_c^m \frac{d_c v_c}{(1 - d_c v_c)} n_c$$

The uptake solutions given conservation of mass $V_m n_m^0 = V_m n_m + N_c v_c n_c$ are:

$$n_m^u(t) = \frac{n_m^0}{(d_c^u v_c k_m^c + k_c^m)} [d_c^u v_c k_m^c e^{-(k_m^c v_c d_c^u + k_c^m)t} + k_c^m], \qquad n_c^u(t) = n_m^0 \frac{(1 - d_c^u v_c) k_m^c}{(d_c^u v_c k_m^c + k_c^m)} [1 - e^{-(k_m^c v_c d_c^u + k_c^m)t}]$$

$$a_m(t) = 1 \times 10^{-3} \lambda N_A \rho_m^{-1} e^{-\lambda t} \begin{cases} n_m^u(t) & 0 \le t \le t_u \\ n_m^e(t) & t > t_u \end{cases}, \qquad a_c(t) = 1 \times 10^{-3} \lambda N_A \rho_c^{-1} e^{-\lambda t} \begin{cases} n_c^u(t) & 0 \le t \le t_u \\ n_c^e(t) & t > t_u \end{cases}$$

$$a_m^u(t) = \frac{a_m^0}{(d_c^u v_c k_m^c + k_c^m)} [d_c^u v_c k_m^c e^{-(k_m^c v_c d_c^u + k_c^m)t} + k_c^m] e^{-\lambda t}, \qquad a_c^u(t) = a_m^0 \frac{(1 - d_c^u v_c) k_m^c}{(d_c^u v_c k_m^c + k_c^m)} [1 - e^{-(k_m^c v_c d_c^u + k_c^m)t}] e^{-\lambda t}$$

$$\tilde{a}_m^u = a_m^0 \left[\frac{k_m^c d_c^u v_c (1 - e^{-(k_m^c d_c^u v_c + k_c^m + \lambda) t_u})}{(k_m^c d_c^u v_c + k_c^m)(k_m^c d_c^u v_c + k_c^m + \lambda)} + \frac{k_c^m (1 - e^{-\lambda t_u})}{\lambda (k_m^c d_c^u v_c + k_c^m)} \right]$$

$$\tilde{a}_c^u = \frac{a_m^0 k_m^c (1 - d_c^u v_c)}{(k_m^c d_c^u v_c + k_c^m)(k_m^c d_c^u v_c + k_c^m + \lambda)\lambda}\left[(k_m^c d_c^u v_c + k_c^m) + \lambda e^{-(k_m^c d_c^u v_c + k_c^m + \lambda)t_u} - (k_m^c d_c^u v_c + k_c^m + \lambda)e^{-\lambda t_u}\right]$$

The efflux solutions given conservation of mass $N_c v_c n_c^0 = V_m n_m + N_c v_c n_c$ are:

$$n_m^e(t) = \frac{d_c^e v_c n_c^0}{(1 - d_c^e v_c)} \frac{k_c^m}{(d_c^e v_c k_m^c + k_c^m)}\left[1 - e^{-(k_m^c d_c^e v_c + k_c^m)t}\right], \qquad n_c^e(t) = \frac{n_c^0}{(k_m^c d_c^e v_c + k_c^m)}\left[k_c^m e^{-(k_m^c d_c^e v_c + k_c^m)t} + k_m^c d_c^e v_c\right]$$

$$a_m^e(t) = \frac{d_c^e v_c a_c^0}{(1 - d_c^e v_c)} \frac{k_c^m}{(d_c^e v_c k_m^c + k_c^m)}\left[1 - e^{-(k_m^c d_c^e v_c + k_c^m)t}\right]e^{-\lambda t}, \qquad a_c^e(t) = \frac{a_c^0}{(k_m^c d_c^e v_c + k_c^m)}\left[k_c^m e^{-(k_m^c d_c^e v_c + k_c^m)t} + k_m^c d_c^e v_c\right]e^{-\lambda t}$$

$$\tilde{a}_m^e = \frac{a_c^0 d_c^e v_c k_c^m}{\lambda(1 - d_c^e v_c)(d_c^e v_c k_m^c + k_c^m + \lambda)} \qquad \tilde{a}_c^e = \frac{a_c^0(\lambda + k_m^c d_c^e v_c)}{\lambda(d_c^e v_c k_m^c + k_c^m + \lambda)}$$

Residence times:

$$\tau_m = \frac{\tilde{a}_m}{a_m^0} = \frac{\tilde{a}_m^u + \tilde{a}_m^e}{a_m^0} = \left[\begin{array}{l} \dfrac{k_m^c d_c^u v_c (1 - e^{-(k_m^c d_c^u v_c + k_c^m + \lambda)t_u})}{(k_m^c d_c^u v_c + k_c^m)(k_m^c d_c^u v_c + k_c^m + \lambda)} + \dfrac{k_c^m (1 - e^{-\lambda t_u})}{\lambda(k_m^c d_c^u v_c + k_c^m)} + \\ \qquad \dfrac{(1 - d_c^u v_c) k_m^c (1 - e^{-(k_m^c v_c d_c^u + k_c^m)t_u}) e^{-\lambda t_u}}{(d_c^u v_c k_m^c + k_c^m)} \dfrac{d_c^e v_c k_c^m}{\lambda(1 - d_c^e v_c)(d_c^e v_c k_m^c + k_c^m + \lambda)} \end{array}\right]$$

$$\tau_c = \frac{\tilde{a}_c}{a_m^0} = \frac{\tilde{a}_c^u + \tilde{a}_c^e}{a_m^0} = \left[\begin{array}{l} \dfrac{k_m^c (1 - d_c^u v_c)\left[(k_m^c d_c^u v_c + k_c^m) + \lambda e^{-(k_m^c d_c^u v_c + k_c^m + \lambda)t_u} - (k_m^c d_c^u v_c + k_c^m + \lambda)e^{-\lambda t_u}\right]}{(k_m^c d_c^u v_c + k_c^m)(k_m^c d_c^u v_c + k_c^m + \lambda)\lambda} + \\ \qquad \dfrac{(1 - d_c^u v_c) k_m^c \left[1 - e^{-(k_m^c d_c^u v_c + k_c^m)t_u}\right] e^{-\lambda t_u}}{(d_c^u v_c k_m^c + k_c^m)} \dfrac{(\lambda + k_m^c d_c^e v_c)}{\lambda(d_c^e v_c k_m^c + k_c^m + \lambda)} \end{array}\right]$$

APPENDIX B

Glossary

n_m Average halide concentration in medium (mol/L)
n_m^u Average halide concentration in medium during uptake (mol/L)
n_m^e Average halide concentration in medium during efflux (mol/L)
n_c Average halide concentration in cells (mol/L)
n_c^u Average halide concentration in cells during uptake (mol/L)
n_c^e Average halide concentration in cells during efflux (mol/L)
V_{max} Theoretical maximum halide transfer rate (mol/L s^{-1})
K_m Michaelis–Menten constant for NIS (mol/L)
v_c Average volume of a cell (cm^{-3})
d_c Average cell density (cell cm^{-3})
d_c^u Average cell density during uptake (cell cm^{-3})
d_c^e Average cell density during efflux (cell cm^{-3})
N_c Total number of cells (cell)
k_c^m Transfer rate between a cell to medium (s^{-1})
k_m^c Transfer rate between medium to a cell (s^{-1})
V_m Volume of medium (cm^3)
V_c Volume of cells (cm^3)
V_T Total volume of system (cm^3)
V_T^u Total volume of system during uptake period (cm^3)
V_T^e Total volume of system during efflux period (cm^3)
$F(d_c)$ Fractional cell uptake (unitless)
$FCAA$ Fractional cell-associated activity (unitless)
a_m Average activity concentration in medium (Bq cm^{-3})
$\tilde{a}_m^u$ Average cumulated activity concentration in medium during uptake (Bq s cm^{-3})
$\tilde{a}_m^e$ Average cumulated activity concentration in medium during efflux (Bq s cm^{-3})
a_c Average activity concentration in the cell (Bq cm^{-3})
$\tilde{a}_c^u$ Average cumulated activity concentration in a cell during uptake (Bq s cm^{-3})
$\tilde{a}_c^e$ Average cumulated activity concentration in a cell during efflux (Bq s cm^{-3})
$\tilde{q}_c$ Average cumulated activity in a cell (Bq s)
τ^u Residence time of system during uptake (s)
τ^e Residence time of system during efflux (s)
τ_m^u Residence time of halide in medium during uptake (s)

τ_c^u Residence time of halide in cells during uptake (s)

τ_m^e Residence time of halide in medium during efflux (s)

τ_c^e Residence time of halide in cells during efflux (s)

D Average absorbed dose (Gy)

$S(m \rightarrow c)$ Dose conversion factor from medium (source) to cells (target) (Gy g Bq^{-1} s^{-1})

$S(c \rightarrow c)$ Dose conversion factor from cells (source) to cells (target) (Gy g Bq^{-1} s^{-1})

h_m^c Average number of hits from medium (source) to a cell (target) (hit)

h_c^c Average number of hits from cells (source) to a cell (target) (hit)

$\bar{z}_{1m}^c$ Specific energy per event from medium (source) to a cell (target) (Gy hit^{-1})

$\bar{z}_{1c}^c$ Specific energy per event from cells (source) to a cell (target) (Gy hit^{-1})

SF Survival fraction (unitless)

SF_2 2-Gy survival fraction (unitless)

λ Physical decay constant of radionuclide (s^{-1})

D_0 Absorbed dose required to reduce survival fraction to e^{-1} (Gy)

A_0 Activity concentration required to reduce survival fraction to e^{-1} (MBq cm^{-3})

REFERENCES

1. Filetti S, Bidart JM, Arturi F, et al. Sodium/iodide symporter: a key transport system in thyroid cancer cell metabolism. *Eur J Endocrinol.* 1999;141:443–457.
2. Chung JK. Sodium iodide symporter: its role in nuclear medicine. *J Nucl Med.* 2002;43:1188–1200.
3. Mandell RB, Mandell LZ, Link CJ Jr. Radioisotope concentrator gene therapy using the sodium/iodide symporter gene. *Cancer Res.* 1999;59:661–668.
4. Carlin S, Cunningham SH, Boyd M, et al. Experimental targeted radioiodide therapy following transfection of the sodium iodide symporter gene: effect on clonogenicity in both two- and three-dimensional models. *Cancer Gene Ther.* 2000;7:1529–1536.
5. Shimura H, Haraguchi K, Miyazaki A, et al. Iodide uptake and experimental ^{131}I therapy in transplanted undifferentiated thyroid cancer cells expressing the Na^+/I^- symporter gene. *Endocrinology.* 1997;138:4493–4496.
6. Boland A, Magnon C, Filetti S, et al. Transposition of the thyroid iodide uptake and organification system in nonthyroid tumor cells by adenoviral vector-mediated gene transfers. *Thyroid.* 2002;12:19–26.
7. Hall EJ. *Radiobiology for the Radiologist.* 3rd ed. Philadelphia, PA: JB Lippincott; 1988.
8. Spitzweg C, O'Connor MK, Bergert ER, et al. Treatment of prostate cancer by radioiodine therapy after tissue-specific expression of the sodium iodide symporter. *Cancer Res.* 2000;60:6526–6530.
9. Nakamoto Y, Saga T, Misaki T, et al. Establishment and characterization of a breast cancer cell line expressing Na^+/I^- symporters for radioiodide concentrator gene therapy. *J Nucl Med.* 2000;41:1898–1904.
10. Cho JY, Shen DH, Yang W, et al. In vivo imaging and radioiodine therapy following sodium iodide symporter gene transfer in animal model of intracerebral gliomas. *Gene Ther.* 2002;9:1139–1145.
11. O'Donoghue JA, Bardies M, Wheldon TE. Relationships between tumor size and curability for uniformly targeted therapy with beta-emitting radionuclides. *J Nucl Med.* 1995;36:1902–1909.
12. Larsen RH, Slade S, Zalutsky MR. Blocking [^{211}At]astatide accumulation in normal tissues: preliminary evaluation of seven potential compounds. *Nucl Med Biol.* 1998;25:351–357.
13. Smit JW, Schroder-van der Elst JP, Karperien M, et al. Iodide kinetics and experimental ^{131}I therapy in a xenotransplanted human sodium-iodide symporter-transfected human follicular thyroid carcinoma cell line. *J Clin Endocrinol Metab.* 2002;87:1247–1253.
14. Dadachova E, Bouzahzah B, Zuckier LS, et al. Rhenium-188 as an alternative to iodine-131 for treatment of breast tumors expressing the sodium/iodide symporter (NIS). *Nucl Med Biol.* 2002;29:13–18.
15. Kampf G. Induction of DNA double-strand breaks by ionizing radiation of different quality and their relevance for cell inactivation. *Radiobiol Radiother (Berl).* 1988;29:631–658.
16. Carlin S, Mairs RJ, Welsh P, et al. Sodium-iodide symporter (NIS)-mediated accumulation of [^{211}At]astatide in NIS-transfected human cancer cells. *Nucl Med Biol.* 2002;29:729–739.
17. Akabani G. Absorbed dose calculations in Haversian canals for several beta-emitting radionuclides. *J Nucl Med.* 1993;34:1361–1366.
18. Akabani G, Hawkins WG, Eckblade MB, et al. Patient-specific dosimetry using quantitative SPECT imaging and three-dimensional discrete Fourier transform convolution. *J Nucl Med.* 1997;38:308–314.
19. Akabani G, Poston JW Sr. Absorbed dose calculations to blood and blood vessels for internally deposited radionuclides. *J Nucl Med.* 1991;32:830–834.
20. Akabani G, Kennel SJ, Zalutsky MR. Microdosimetric analysis of α-particle-emitting targeted radiotherapeutics using histological images. *J Nucl Med.* 2003; 44:792–805.
21. Petrich T, Helmeke HJ, Meyer GJ, et al. Establishment of radioactive astatine and iodine uptake in cancer cell lines expressing the human sodium/iodide symporter. *Eur J Nucl Med Mol Imaging.* 2002;29:842–854.
22. Strickland DK, Vaidyanathan G, Zalutsky MR. Cytotoxicity of alpha-particle-emitting m-[^{211}At]astatobenzylguanidine on human neuroblastoma cells. *Cancer Res.* 1994;54:5414–5419.
23. Humm JL. A microdosimetric model of astatine-211 labeled antibodies for radioimmunotherapy. *Int J Radiat Oncol Biol Phys.* 1987;13:1767–1773.
24. Min JJ, Chung JK, Lee YJ, et al. In vitro and in vivo characteristics of a human colon cancer cell line, SNU-C5N, expressing sodium-iodide symporter. *Nucl Med Biol.* 2002;29:537–545.
25. La Perle KM, Shen D, Buckwalter TL, et al. In vivo expression and function of the sodium iodide symporter following gene transfer in the MATLyLu rat model of metastatic prostate cancer. *Prostate.* 2002;50:170–178.
26. Moon DH, Lee SJ, Park KY, et al. Correlation between ^{99m}Tc-pertechnetate uptakes and expressions of human sodium iodide symporter gene in breast tumor tissues. *Nucl Med Biol.* 2001;28:829–834.
27. Groot-Wassink T, Aboagye EO, Glaser M, et al. Adenovirus biodistribution and noninvasive imaging of gene expression in vivo by positron emission tomography using human sodium/iodide symporter as reporter gene. *Hum Gene Ther.* 2002; 13:1723–1735.
28. Zalutsky MR, Vaidyanathan G. Astatine-211-labeled radiotherapeutics: an emerging approach to targeted alpha-particle radiotherapy. *Curr Pharm Des.* 2000;6:1433–1455.
29. Cobb LM, Harrison A, Dudley NE, et al. Relative concentration of astatine-211 and iodine-125 by human fetal thyroid and carcinoma of the thyroid in nude mice. *Radiother Oncol.* 1988;13:203–209.
30. Brown I, Carpenter RN. Endogenous ^{211}At alpha-particle radiotherapy for undifferentiated thyroid cancer. *Acta Radiol Suppl.* 1991;376:174–175.
31. Lazar V, Bidart JM, Caillou B, et al. Expression of the Na^+/I^- symporter gene in human thyroid tumors: a comparison study with other thyroid-specific genes. *J Clin Endocrinol Metab.* 1999;84:3228–3234.
32. Lindencrona U, Nilsson M, Forssell-Aronsson E. Similarities and differences between free ^{211}At and ^{125}I-transport in porcine thyroid epithelial cells cultured in bicameral chambers. *Nucl Med Biol.* 2001;28:41–50.
33. Hamilton JG AC, Garrison WM, Scott KG. The accumulation, metabolism and biological effects of astatine in rats and monkeys. In: TDa WE, Anderson HH, eds. *University of California Publications in Pharmacology.* Vol. 2. Los Angeles, CA: University of California Press; 1953:283–344.